applied optics

Surface defect detection method for glass substrate using improved Otsu segmentation

ZHIYONG HE* AND LINING SUN

School of Mechanical and Electric Engineering, Soochow University, Suzhou 215021, China
**Corresponding author: hezhiyong@suda.edu.cn*

Received 25 August 2015; revised 6 October 2015; accepted 17 October 2015; posted 20 October 2015 (Doc. ID 248586); published 16 November 2015

The image quality degradation caused by noise makes the automatic optical inspection of surface defects difficult. This paper develops a method based on thresholding segmentation to detect the surface defects in a glass substrate. Traditional Otsu segmentation has poor anti-noise ability. In order to improve the traditional Otsu method, a straight-line intercept histogram is established directly from the two-dimensional information of an image, and then Otsu criteria can be used to find the best intercept threshold from the one-dimensional histogram established. The improved Otsu algorithm not only is simpler than the two-dimensional Otsu methods, but also has a robust anti-noise ability. In the surface defect detection, the contrast feature between object and background is simply extracted after the segmentation based on the improved Otsu method, and surface defects can be decided by the threshold of the contrast feature. The data used in the experiments include the surface images acquired by a line-scan CCD camera. The experimental results demonstrate that the proposed method is effective and computationally efficient.

OCIS codes: (120.4630) Optical inspection; (150.1135) Algorithms; (150.1835) Defect understanding; (100.2960) Image analysis; (100.3008) Image recognition, algorithms and filters.

http://dx.doi.org/10.1364/AO.54.009823

1. INTRODUCTION

The automatic optical inspection of surface defects is very important for ensuring a product's quality. Thresholding is widely used in surface defect detection [1–7]. Because there is no complex background texture in the surface image of a glass substrate, it is important and feasible to segment defects directly using the thresholding technique. Based on feature extraction, the thresholding technique also can be applied in finding a surface defect from the segmentation result.

Noise, non uniform illumination, and the variance of the relative illumination curve of a lens will cause the quality degradation of a surface image in surface defect detection in a glass substrate, and the degradation will make image segmentation challenging.

In the algorithms of image segmentation, thresholding is simple and fast [8]. As a classic thresholding method, the Otsu method [9] is adaptive and effective, and is widely used in image segmentation [8,10,11,12]. The Otsu method can obtain a stable segmentation quality, so it is commonly used in the detection of surface defects [5,6]. As a simple method that is based on a one-dimensional (1D) gray histogram and the maximum between-class variance rule, the Otsu method sometimes cannot produce a satisfactory result. For accurate segmenting, some methods have been proposed to improve the Otsu method, such as the methods in [7,13–22].

When an image is polluted by noise, the traditional Otsu method has a poor effect on image segmentation. Two-dimensional (2D) Otsu methods [16–21] have better anti-noise ability than the traditional Otsu method. The 2D Otsu methods establish a 2D histogram based on the intensity value and mean intensity value of the neighborhood, then compute a 2D threshold based on the 2D histogram, but the computation of the method is highly complex.

In order to improve the Otsu method, we use the 2D information of a pixel to directly establish a 1D histogram, which is called the straight-line intercept histogram. Otsu criteria can be applied in solving the optimal intercept threshold, which is applied in thresholding segmentation [15]. The analysis of the measurement of the between-class discrete degree shows that the improved Otsu method can effectively resist noise, while the computational complexity of the algorithm is lower than any 2D Otsu method.

Based on the improved Otsu method, a new surface defect detection method for glass substrates is presented. In the method, the surface defect detection can be accomplished only by extracting and comparing the contrast feature between the

target region and the background. The new method can resist noise and is computationally efficient. In the experiment, the surface image of the glass substrate was acquired by a line-scan CCD camera, and the image was analyzed. The experimental results show the effectiveness and computational efficiency of the proposed method in surface defect detection in a glass substrate.

2. IMPROVED OTSU SEGMENTATION

A. Straight-Line Intercept Histogram

For an image whose intensity level is L, the intensity value of the pixel and the mean intensity value of the neighborhood can be composed and represented as (i, j). In the following equation, f_{ij} represents the frequency of (i, j) in image, N is the total number of pixels in the image, and p_{ij} is the probability density of (i, j) in the image:

$$p_{ij} = f_{ij}/N, \tag{1}$$

where $\Sigma_{i=0}^{L-1}\Sigma_{j=0}^{L-1}p_{ij} = 1$.

The histogram defined by Eq. (1) is called a 2D histogram. The equation $i + j = k$ represents the straight line, which is perpendicular to the main diagonal vertical, and the intercept of the straight line is k. There are $2L$ straight lines that are perpendicular to the main diagonal line in a 2D histogram.

If f_k is the frequency of (i, j), which meets the condition $i + j = k$, then the probability density of the pixels that meet the condition of $i + j = k$ is:

$$p_k = \sum_{i+j=k} p_{ij} = fk/N, \qquad k = 0, 1, \ldots, 2L - 1, \tag{2}$$

where $\Sigma_{k=0}^{2L-1} p_k = 1$. The histogram defined by the above methods is called a straight-line intercept histogram.

The straight-line intercept histogram of Lena is shown in Fig. 1.

B. Thresholding Segmentation

When segmenting, a 2D histogram using the straight line that is perpendicular to the main diagonal. The threshold straight line can be uniquely decided by the intercept of the straight line. Here, T indicates the intercept of the straight-line threshold. The essence of finding the best straight-line threshold is to determine the optimal intercept threshold T^*, and the solving process can be based on the Otsu criteria and the straight-line intercept histogram.

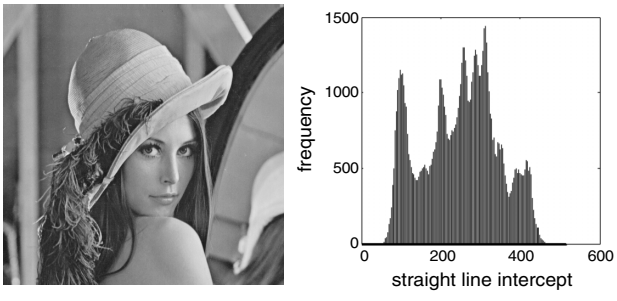

(a) (b)

Fig. 1. (a) Lena and (b) straight-line intercept histogram of Lena.

By using threshold T, all straight-line intercepts in the histogram can be divided into two class: $C_0(T)$ and $C_1(T)$, where $C_0(T) = [0, \ldots, T]$ and $C_1(T) = [T + 1, \ldots, 2L - 1]$. The mean values of $C_0(T)$ and $C_1(T)$ are, respectively, denoted as $\mu_0(T)$ and $\mu_1(T)$. If $\omega_0(T) = \Sigma_{k=0}^{T} p_k$, $\omega_1(T) = 1 - \omega_0(T)$, $\mu(T) = \Sigma_{k=0}^{T} k p_k$, and $\mu_T = \Sigma_{k=0}^{2L-1} k p_k$, then:

$$\mu_0(T) = \sum_{k=0}^{T} k p_k/\omega_0(T) = \mu(T)/\omega_0(T), \tag{3}$$

$$\mu_1(T) = \sum_{k=T+1}^{2L-1} k p_k/\omega_1(T) = \frac{\mu_T - \mu(T)}{1 - \omega_0(T)}. \tag{4}$$

Between-class variance σ_B^2 can be computed using

$$\begin{aligned}\sigma_B^2(T) &= \omega_0(T)[\mu_0(T) - \mu_T]^2 + \omega_1(T)[\mu_1(T) - \mu_T]^2 \\ &= \omega_0(T)\omega_1(T)[\mu_0(T) - \mu_1(T)]^2.\end{aligned} \tag{5}$$

The optimal threshold T^* can be selected from

$$\sigma_B^2(T^*) = \max_{0 \le T < 2L-1} \sigma_B^2(T). \tag{6}$$

After T^* is obtained, all pixels can be classified using

$$f(x, y) = \begin{cases} 0 & \text{if } i + j \le T^* \\ L - 1 & \text{if } i + j > T^* \end{cases}, \tag{7}$$

where $f(x, y)$ is the segmented image.

C. Performance analysis

1. Anti-Noise Ability

Suppose there is target region C_0 and background region C_1 in the 2D histogram. Then, the probabilities of C_0 and C_1, respectively, are:

$$\omega_0 = \sum_{(i,j)\in C_0} p_{ij}, \tag{8}$$

$$\omega_1 = \sum_{(i,j)\in C_1} p_{ij}. \tag{9}$$

The mean value vectors of the two classes are:

$$\boldsymbol{\mu}_0 = (\mu_{0i}, \mu_{0j})^T = \left(\sum\nolimits_{(i,j)\in C_0} i p_{ij}/\omega_0, \sum_{(i,j)\in C_0} j p_{ij}/\omega_0 \right)^T, \tag{10}$$

$$\boldsymbol{\mu}_0 = (\mu_{1i}, \mu_{1j})^T = \left(\sum\nolimits_{(i,j)\in C_1} i p_{ij}/\omega_1, \sum_{(i,j)\in C_1} j p_{ij}/\omega_1 \right)^T. \tag{11}$$

We define d as follows:

$$d = \sqrt{[(\mu_{0i} - \mu_{1i})^2 + (\mu_{0j} - \mu_{1j})^2]}, \tag{12}$$

where d denotes the distance between the mean value point of C_0 and the mean value point of C_1 in the 2D histogram.

If an image is not polluted by noise, the probability distribution of the image in the 2D histogram is mainly concentrated in the main diagonal, because the intensity value of the pixel is usually close to the mean intensity value of the neighborhood.

For any intercept threshold T, a straight-line threshold $i + j = T$ can be generated in a 2D histogram. Using the threshold, the 2D histogram can be divided into two region: $0 \le i + j \le T$ and $T < i + j \le 2L - 1$, respectively, denoted as C_0 and C_1. Consider Eqs. (8) and (9). We get:

$$\omega_0(T) = \sum_{k=0}^{T} p_k = \sum_{i+j=0}^{T} p_{ij} = \sum_{(i,j)\in C_0} p_{ij} = \omega_0, \quad (13)$$

$$\omega_1(T) = \sum_{k=T+1}^{2L-1} p_k = \sum_{i+j=T+1}^{2L-1} p_{ij} = \sum_{(i,j)\in C_1} p_{ij} = \omega_1. \quad (14)$$

By combining Eqs. (13), (14), and (10), $\mu_0(T)$ can be rewritten as

$$\begin{aligned}\mu_0(T) &= \sum_{k=0}^{T} k p_k/\omega_0(T) = \sum_{i+j=0}^{T} (i+j)p_{ij}/\omega_0(T)\\ &= \sum_{(i,j)\in C_0} (i+j)p_{ij}/\omega_0\\ &= \sum_{(i,j)\in C_0} i p_{ij}/\omega_0 + \sum_{(i,j)\in C_0} j p_{ij}/\omega_0 = \mu_{0i} + \mu_{0j}. \quad (15)\end{aligned}$$

Similarly, there is

$$\mu_1(T) = \mu_{1i} + \mu_{1j}. \quad (16)$$

Further, there is

$$\begin{aligned}\sigma_B^2(T) &= \omega_0(T)\omega_1(T)[\mu_0(T) - \mu_1(T)]^2\\ &= \omega_0\omega_1[(\mu_{0i} - \mu_{1i})^2\\ &\quad + (\mu_{0j} - \mu_{1j})^2 + 2(\mu_{0i} - \mu_{1i})(\mu_{0j} - \mu_{1j})]. \quad (17)\end{aligned}$$

The definition of d is same as Eq. (12), and the definition of θ in the 2D histogram is shown in Fig. 2. We get:

$$\mu_{1j} - \mu_{0j} = d\cos\theta, \quad (18)$$

$$\mu_{1i} - \mu_{0i} = d\sin\theta. \quad (19)$$

By combining Eqs. (12), (18), and (19) with Eq. (17), we get:

$$\sigma_B^2(T) = \omega_0\omega_1 d^2(1 + \sin 2\theta). \quad (20)$$

In Eq. (20), the value of $(1 + \sin 2\theta)$ will be at its maximum when $\theta = 45°$, which means the maximum of $\sigma_B^2(T)$ will be easily obtained when the straight line between the mean value point of C_0 and the mean value point of C_1 is close to the main diagonal of the 2D histogram, so the thresholding has the anti-noise ability.

2. Computational Complexity

Both in the establishment of the straight-line intercept histogram and in the establishment of the 2D histogram, it is necessary to traverse the 2D information of all the pixels. The proposed algorithm computes the probability density $2L$ times, and the 2D Otsu method needs to compute probability density L^2 times.

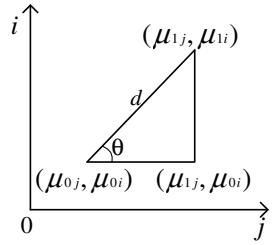

Fig. 2. Definition of θ in 2D histogram.

Our algorithm to obtain the optimal threshold only needs to compute the between-class variance in the 1D histogram, which is based on the $2L$ space. The analysis in [17] shows that the computational complexity of the 2D Otsu method in [17] is lower than 2D Otsu methods in [15,16]. But the method in [17] needs to traverse the L^2 space not only in computing Σp_{ij}, $\Sigma i p_{ij}$, and $\Sigma j p_{ij}$ for each threshold, it also needs to compute the trace of the between-class difference matrix.

3. PROPOSED DEFECT DETECTION METHOD

A. Feature Extraction

After effectively segmenting the image by using the improved Otsu method, it can be decided whether the segmented target region is a surface defect region. For a segmented image, we extract the feature based on the contrast between the target and background, and the feature is defined as follows:

$$C = \left|\frac{\mu_{\mathrm{Obj}} - \mu_{\mathrm{Bkg}}}{\mu_{\mathrm{Obj}} + \mu_{\mathrm{Bkg}}}\right|. \quad (21)$$

In Eq. (21), μ_{Obj} and μ_{Bkg}, respectively, denote the mean intensity values in the target area and in the background area.

Because of the uniformity of the glass surface, the contrast between the target region and the background will be large if the defects are located in the target region; otherwise, the contrast will be relatively small. Whether the target region is a surface defect region can be decided according to the principle above.

B. Defect Detection Algorithm for Glass Substrate

If the surface image of a glass substrate is polluted by noise, our improved Otsu method can be applied to segment the image; if the surface image is simultaneously influenced by the non uniform illumination and noise, we can divide the image into many sub-images first, and then our improved Otsu method can be applied for each sub-image.

According to the magnitude of feature C, we can find the defective image. In applications, the supervised thresholding algorithm can be used to detect surface defects as follows:

(1) Construct a sample image group. The sample image group includes a set of defective images and a set of defect-free images.

(2) Segment images in sample image group by the improved Otsu method.

(3) Extract feature C of images in sample image group by using Eq. (21) and by comparing the features of two sets. Select one threshold Thr for feature classification following this such criterion: Thr should classify two sets with minimum error times.

(4) Segment the surface image which should be detected by the improved Otsu method.

(5) Extract feature C of the surface image, which should be detected by using Eq. (21).

(6) Find the threshold for the surface image: if $C > Thr$, then the image is defective; otherwise, a surface defect does not exist in the target region.

Threshold selection for detection is finished in steps (1)–(3). The feature is usually obviously different between the defective image and defect-free image, so the threshold Thr is usually easy to select. When detecting, the algorithm only needs to

perform steps (4)–(6). So, the whole computation process is simple enough to meet the real-time requirements of online detection.

4. EXPERIMENTAL RESULTS

The experiments are conducted on a computer using MATLAB R2010a, with Intel Core i5-4210u CPU and 4 GB of memory.

In order to evaluate the improvement of the anti-noise ability by our improved Otsu method, we compared the traditional Otsu method and the 2D Otsu method with our improved Otsu method. In our experiment, the neighborhood of 3×3 is used to compute the mean intensity value for each pixel, both in the 2D Otsu method and in our improved Otsu method. Gaussian noise is added to some clear images, and these images are segmented using the different methods. Figure 3 shows some examples of the segmentation results.

It is also very important to objectively evaluate the anti-noise performance of different segmentation algorithms. In the evaluation, the results segmented from the clear images by using the traditional Otsu method are looked upon as the ideal segmentation results, and the results obtained from the images polluted by noise are looked upon as the real segmentation results.

In the real segmentation results, one pixel is positive if it is segmented as one target pixel; otherwise, the pixel is negative. The real segmentation result of one pixel is called true if it is same as the ideal segmentation result of the pixel; otherwise, the real segmentation result is false.

In order to compare the precision of the segmentation results, we compute True Positive Rate (*TPR*) and False Detection Rate (*FDR*) based on the number of *TP* (true positive) pixels, the number of *FN* (false negative) pixels, the number of *TN* (true negative) pixels, and the number of *FP* (false positive) pixels. *TPR* can be obtained using Eq. (22), and *TNR* can be obtained using Eq. (23):

$$TPR = \frac{TP}{TP + FN}, \tag{22}$$

$$TNR = \frac{TN}{TN + FP}. \tag{23}$$

where *TPR* represents the ratio of the target pixels segmented correctly to all target pixels, while *TNR* represents the ratio of the background pixels segmented correctly to all background pixels. If both the *TPR* and *TNR* are large, the real segmentation is close to the ideal segmentation, and the anti-noise performance of the real segmentation algorithm is better. Table 1 shows the experimental results described by the *TPR* and *TNR*.

Figure 3 and Table 1 show that the improved Otsu method can achieve more precise results than the traditional Otsu method and the 2D Otsu method when the segmented images are polluted by noise.

In our defect detection experiments, the image acquisition hardware system includes the DALSA P2-04K40 industrial line-scan CCD, Schneider Componon APO 4.0/60 lens, and the DALSA X64CL-iPro image acquisition board. The image acquisition device is shown in Fig. 4.

In the experiments, the illumination pattern we used is a dark field. When the dark-field pattern works, most lights will pass through transparent glass substrate, and the lights that reach the defect region can be reflected to the CCD. The surface image example acquired in this pattern is shown in

Table 1. *TPR* and *TNR* of Segmentation Methods (Deviation of Added Gaussian Noise is 0.006)

Image name		Noisy Lena	Noisy Circuit	Noisy Rice
Traditional Otsu	*TPR*	0.8817	0.9528	0.9531
	TNR	0.9058	0.9742	0.8802
	average of *TPR* and *TNR*	0.8937	0.9635	0.9166
2D Otsu	*TPR*	0.9276	0.9865	0.9459
	TNR	0.9254	0.9783	0.9537
	average of *TPR* and *TNR*	0.9265	0.9824	0.9498
Improved Otsu	*TPR*	0.9252	0.9845	0.9542
	TNR	0.9514	0.9848	0.9673
	average of *TPR* and *TNR*	0.9383	0.98465	0.96075

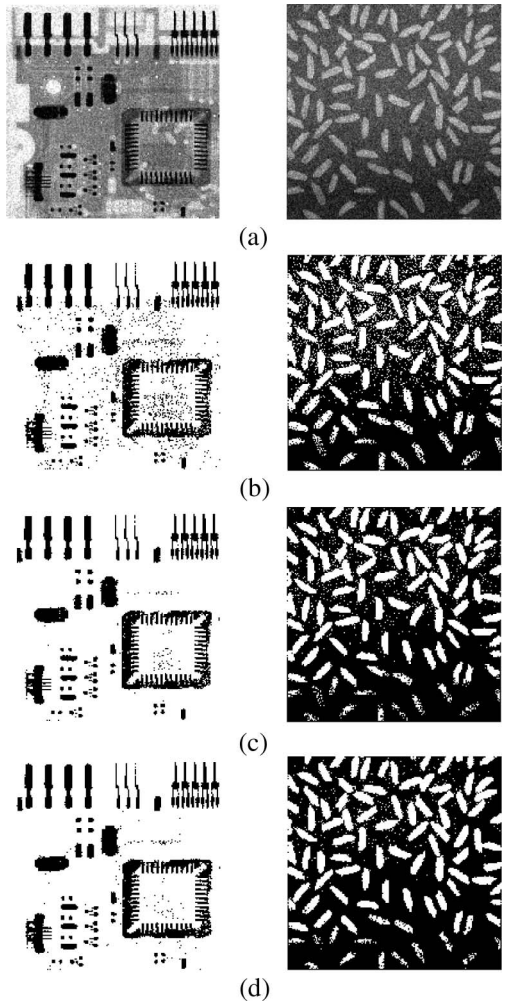

Fig. 3. Examples for comparison of segmentation methods (deviation of added Gaussian noise is 0.006). (a) Noisy images. (b) Segmentation results by using traditional Otsu. (c) Segmentation results by using 2d Otsu [16,17]. (d) Segmentation results by using improved Otsu.

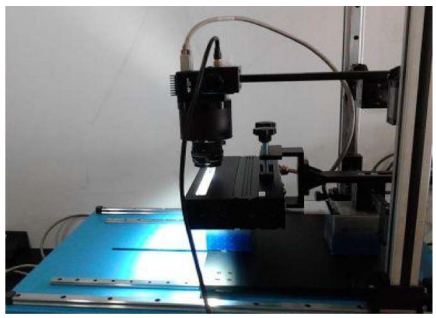

Fig. 4. Image acquisition device for glass substrate surface.

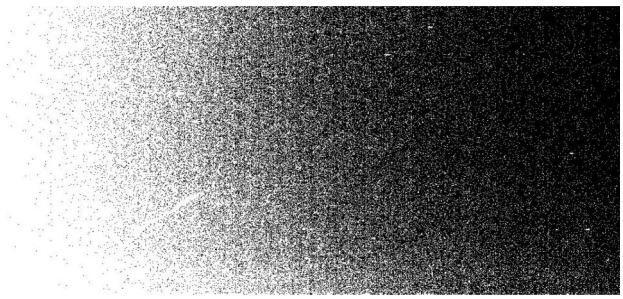

Fig. 6. Segmentation result by using traditional Otsu method on whole image.

Fig. 5. Because of the dark-field pattern, the defect is bright and the background is dark, as shown in Fig. 5.

The dataset used in the defect detection experiment is the glass substrate surface images acquired. Noise and non uniform illumination can affect the image quality, and sometimes they happen in the image simultaneously. Figure 5 shows some surface defects, such as a scratch, a stain, and hair in the surface image of the glass substrate. Although the background of Fig. 5 appears to be uniform, the illumination of the background is in fact slowly changed, and the noise caused by the acquisition system also exists in the image. Noise and non uniform illumination will affect the accuracy of the image segmentation results.

Figure 6 shows the result when directly segmenting the whole image of the glass substrate by the traditional Otsu method. Due to the uneven distribution of the brightness of the glass substrate surface image, the segmentation will lead to a serious error when trying to segment the defects out.

If the whole image is divided into a number of local regions, the background brightness variations within a local region will be small because the illumination change is slow. In that case, more accurate segmentation results should be achieved by using the Otsu method in the local regions, because the Otsu threshold is adaptive. Due to the strategy of dividing the whole image into a number of local regions and performing the Otsu method for each local region, Fig. 7(a) shows better segmentation results than Fig. 6. In Fig. 7, a number of surface defects are detected.

In Fig. 7, one part of the scratch does not appear to be accurately segmented and detected. The reason is that the contrast between the scratch and the background is so small that noise interferes with the segmentation. Similarly, the experimental result in Fig. 8 shows that the detection method using the iterative tri-class thresholding method [22] also cannot produce a satisfactory result.

Figure 9 shows a better experimental result than Figs. 7 and 8, because the 2D Otsu method has the anti-noise ability in segmentation. The algorithm proposed in section 3 is also performed to detect surface defects in the experiments. Figure 10 shows the detection results of Fig. 5 using the proposed detection method. By comparing Fig. 10 with Figs. 7–9, it is clearly seen that our segmentation result and detection result are better than the others.

It is also necessary to objectively evaluate different algorithms. The images used in the evaluation are influenced by non uniform illumination and noise simultaneously. The surface image is divided into 1280 sub-images (each sub-image is 48 pixels × 64 pixels), and 85 of them are defective. In our experiment, 80 normal sub-images and 10 defective sub-images are selected as samples for the selection of feature threshold Thr, and the other images are used as the test group.

When evaluating the accuracy of the detection algorithm, TPR and FDR are also helpful. In the detection results, one

Fig. 5. Surface image of glass substrate.

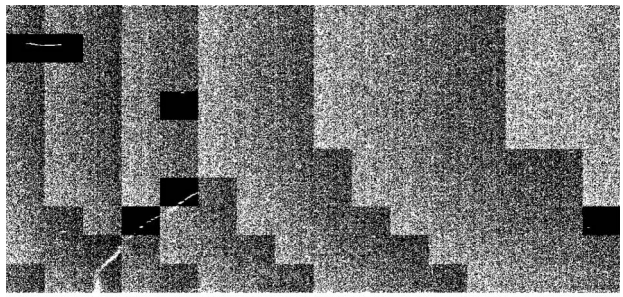

(a)

(b)

Fig. 7. Detection by using traditional Otsu method on sub-images (each sub-image is 48 pixels × 64 pixels). (a) Segmentation result. (b) Detection result.

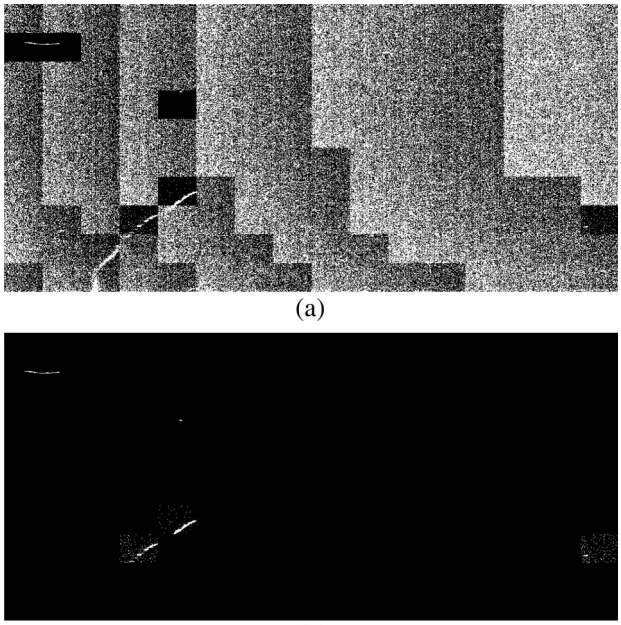

Fig. 8. Detection by using the iterative tri-class thresholding method [22] on sub-images (each sub-image is 48 pixels × 64 pixels). The iteration number is three. (a) Segmentation result. (b) Detection result.

sub-image is positive if it is classified as a defective sub-image. Then, *TPR* and *FDR* can be computed from the number of *TP* sub-images, the number of *FN* sub-images, the number of *TN* sub-images, and the number of *FP* sub-images. The definition of *TPR* has been shown in Eq. (22), and *FDR* can be obtained by performing Eq. (24):

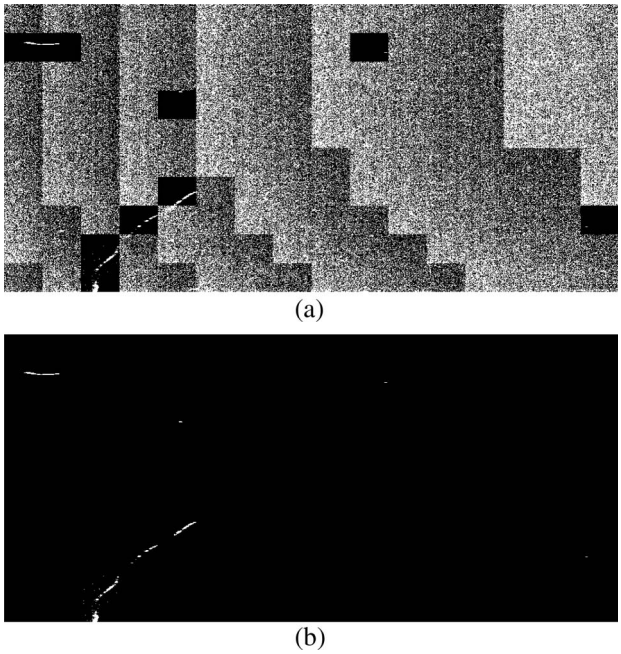

Fig. 9. Detection by using 2D Otsu method on sub-images (each sub-image is 48 pixels × 64 pixels). (a) Segmentation result. (b) Detection result.

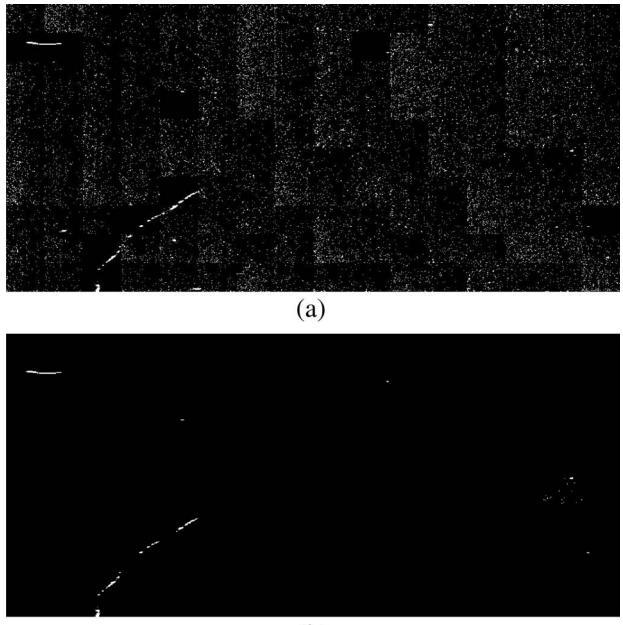

Fig. 10. Detection by using the improved Otsu method on sub-images (each sub-image is 48 pixels × 64 pixels). (a) Segmentation result. (b) Detection result.

$$FDR = \frac{FP}{FP + TP}. \tag{24}$$

In the evaluation, *TPR* represents the algorithm's ability to find defects, and *FDR* indicates the ratio of false defects to the defects found. In the detection, one sub-image is positive if the sub-image is defective.

In order to compare the computational efficiency of our method with other algorithms, we performed each algorithm on the surface image (480 pixels ×1024 pixels) and recorded the execution time for each program in the experiments.

Table 2 shows the experimental results of several methods: one is the detection method proposed in section 3, and the others are different from the proposed method because of the different segmentation algorithms. The experimental results show that the accuracy and the execution time are significantly affected by the segmentation method. The experimental results

Table 2. Performance of Defect Detection

	Thr	TPR	FDR	Time
Detection method proposed	0.09	98.6%	1.3%	0.35 s
Detection method using traditional Otsu in segmentation	0.08	74.6%	0	0.20 s
Detection method using the iterative tri-class thresholding [22] in segmentation	0.075	77.3%	0	0.26 s
Detection method using fast 2D Otsu [17] in segmentation	0.09	96%	1.4%	5.75 s

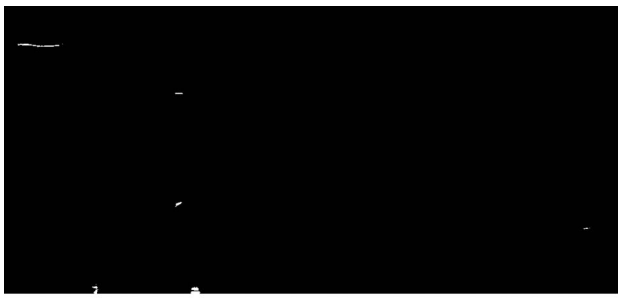

(a)

(b)

Fig. 11. Segmentation result by using the LIF method [24] on whole image. (a) Segmentation result when iteration number is 25. (b) Segmentation result when iteration number is 50.

in Table 2 also show that the proposed detection method based on the improved Otsu method is computationally efficient and more effective.

Beside the several methods compared above, the local image fitting (LIF) method [23] also can be used to segment defects from the background, as shown in Fig. 11. Although the segmentation result achieved by the LIF method will be better when the iteration number is larger, the computation time will also be longer. In the experiment, many defects can be directly separated from the background when the iteration number is 50, but the computation time for one image (480 pixels ×1024 pixels) is 13.9 s.

Because surface defect detection is applied in the high-speed production line of glass substrates, the computational efficiency is very important to the detection. The LIF method [23] is not suitable to segments defects from a glass substrate due to its complex computation. Similarly, the computation method in [24] is too complex for the surface defect detection for a glass substrate, because it uses a watershed as the segmentation algorithm. Compared with the LIF method [23] and the method in [24], our method is more suitable to real-time applications, such as surface defect detection in glass substrates.

5. CONCLUSION

In order to segment a surface polluted by noise, the traditional Otsu method is improved. The improved Otsu method is based on 2D information, but does not establish a 2D histogram. The improved Otsu method segments an image by using Otsu criteria and a 1D straight-line intercept histogram. Both the theoretical analysis and the evaluation results in the experiments show that the algorithm can avoid the disadvantages of the traditional Otsu method in the aspect of anti-noise.

Noise and non uniform illumination will affect the quality of the surface image of a glass substrate. Based on using the improved Otsu method to separate defects from the background, this paper presents a method to decide whether the target region segmented from the surface image of the glass substrate includes a surface defect, and the computation of the proposed method is very simple. The experimental results show that the new detection method is effective and computationally efficient in detecting surface defects in glass substrates.

Funding. National Natural Science Foundation of China (NSFC) (61473201).

REFERENCES

1. A. S. Tolba, "Fast defect detection in homogeneous flat surface products," Expert Syst. Appl. **38**, 12339–12347 (2011).
2. M. Shi, R. Fu, Y. Guo, S. Bai, and B. Xu, "Fabric defect detection using local contrast deviations," Multimedia Tools Appl. **52**, 147–157 (2011).
3. D. M. Tsai and J. Y. Luo, "Mean shift-based defect detection in multicrystalline solar wafer surfaces," IEEE Trans. Indust. Informat. **7**, 125–135 (2011).
4. S. Ghorai, A. Mukherjee, M. Gangadaran, and P. K. Dutta, "Automatic defect detectionon hot-rolled flat steel products," IEEE Trans. Instrum. Meas. **62**, 612–621 (2013).
5. X. W. Zhang, Y. Q. Ding, Y. Y. Lv, A. Y. Shi, and R. Y. Liang, "A vision inspection system for the surface defects of strongly reflected metal based on multi-class SVM," Expert Syst. Appl. **38**, 5930–5939 (2011).
6. Q. Y. Li and S. W. Ren, "A real-time visual inspection system for discrete surface defects of rail heads," IEEE Trans. Instrum. Meas. **61**, 2189–2199 (2012).
7. X. C. Yuan, L. S. Wu, and Q. J. Peng, "An improved Otsu method using the weighted object variance for defect detection," Appl. Surf. Sci. **349**, 472–484 (2015).
8. S. Mehmet and S. Bulent, "Survey over image thresholding techniques and quantitative performance evaluation," J. Electron. Imaging **13**, 146–165 (2004).
9. N. Otsu, "A threshold selection method from gray-level histograms," IEEE Trans. Syst. Man Cybern. **9**, 62–66 (1979).
10. P. K. Sahoo, S. Soltani, A. K. C. Wong, and Y. C. Chen, "A survey of thresholding techniques," Computer Vis. Graph. Image Process. **41**, 233–260 (1988).
11. F. You, R. H. Zhang, L. S. Zhong, H. W. Wang, and J. M. Xu, "Lane detection algorithm for night-time digital image based on distribution feature of boundary pixels," J. Opt. Soc. Korea **17**, 188–199 (2013).
12. S.-J. Kang, S. I. Cho, S. Yoo, and Y. H. Kim, "Scene change detection using multiple histograms for motion-compensated frame rate up-conversion," J. Display Technol. **8**, 121–126 (2012).
13. H. Ng, "Automatic thresholding for defect detection," Pattern Recogn. Lett. **27**, 1644–1649 (2006).
14. F. M. Reza and C. Mohamed, "AdOtsu: An adaptive and parameterless generalization of Otsu's method for document image binarization," Pattern Recogn. **45**, 2419–2431 (2012).
15. Z. Y. He, L. N. Sun, W. G. Huang, and L. G. Chen, "Thresholding segmentation algorithm based on Otsu criterion and line intercept histogram," Opt. Precis. Eng. **20**, 2315–2323 (2012).
16. J. Z. Liu, W. Q. Li, and Y. P. Tian, "Automatic thresholding of gray-level pictures using two-dimension Otsu method," in *IEEE International Conference on Circuits and Systems*, China, 1991, pp. 325–327.
17. H. Y. Wang and D. L. Pan, "A fast algorithm for two-dimensional Otsu adaptive threshold algorithm," Acta Autom. Sin. **33**, 968–971 (2007).
18. Y. Q. Wu, Z. Pan, and W. Y. Wu, "Image thresholding based on two-dimensional histogram oblique segmentation and its fast recurring algorithm," J. Commun. **29**, 77–83 (2008).

19. Q. Chen, L. Zhao, J. Lu, G. Kuang, N. Wang, and Y. Jiang, "Modified two-dimensional Otsu image segmentation algorithm and fast realisation," IET Image Process. **6**, 426–433 (2012).
20. S. Puthipong and S. A. Thitiwan, "A two-stage Otsu's thresholding based method on a 2D histogram," in *IEEE 7th International Conference on Intelligent Computer Communication and Processing*, 2011, pp. 345–348.
21. Y. Li, T. Meng, and A. Li, "Two-dimensional Otsu image segmentation algorithm based on the particle swarm optimization algorithm," in *Future Control and Automation* (Springer, 2012), pp. 115–120.
22. H. M. Cai, Z. Yang, and X. H. Cao, "A new iterative triclass thresholding technique in image segmentation," IEEE Trans. Image Process. **23**, 5497–5509 (2014).
23. K. H. Zhang, H. H. Song, and L. Zhang, "Active contours driven by local image fitting energy," Pattern Recogn. **43**, 1199–1206 (2010).
24. Y. Xie, Y. T. Ye, J. Zhang, L. Liu, and L. Liu, "A physics-based defects model and inspection algorithm for automatic visual inspection," Opt. Lasers Eng. **52**, 218–223 (2014).